

Vision-based Localization and Control of Leader-Follower Formations

Authors:

Gian Luca Mariottini, Fabio Morbidi, Domenico Prattichizzo,
Nicholas Vander Valk, Nathan Michael, George Pappas, Kostas Daniilidis

Gian Luca Mariottini (*Corresponding Author*), Fabio Morbidi and Domenico Prattichizzo,
Dipartimento di Ingegneria dell'Informazione, Università di Siena,
Via Roma 56, 53100 Siena, Italy.

E-mail: {gmariottini,morbidi,prattichizzo}@dii.unisi.it.

Phone: +39 0577 234640,

Fax: +39 0577 233602.

N. Vander Valk, N. Michael, G.J. Pappas and K. Daniilidis,

GRASP Laboratory, University of Pennsylvania,

Philadelphia, PA 19104, USA.

E-mail: {nvander,nmichael}@seas.upenn.edu,pappasg@ee.upenn.edu,kostas@cis.upenn.edu

Abstract:

The paper deals with vision-based localization and control of leader-follower formations of unicycle robots. Each robot is equipped with a panoramic camera which only provides the view-angle to the other robots. As an original contribution, the localization problem is analytically studied using a new observability condition valid for general nonlinear systems and based on the Extended Output Jacobian matrix. The state of the leader-follower system, estimated via the extended Kalman filter, is used by an input-state feedback control law to stabilize the formation. Simulations as well as experimental results validate the theoretical results and show the effectiveness of the proposed design.

Index terms: Mobile robots, nonlinear observability, formation control, panoramic cameras, feedback linearization.

Paper Type:

Short Paper

Vision-based Localization and Control of Leader-Follower Formations

Gian Luca Mariottini, *Memb., IEEE*, Fabio Morbidi, *Student Memb., IEEE*, Domenico Prattichizzo, *Memb., IEEE*, Nicholas Vander Valk, *Student memb., IEEE*, Nathan Michael, *Student memb., IEEE*, George Pappas, *Senior Memb., IEEE*, Kostas Daniilidis, *Senior Memb., IEEE*,

Abstract—The paper deals with vision-based localization and control of leader-follower formations of unicycle robots. Each robot is equipped with a panoramic camera which only provides the view-angle to the other robots. As an original contribution, the localization problem is analytically studied using a new observability condition valid for general nonlinear systems and based on the Extended Output Jacobian matrix. The state of the leader-follower system, estimated via the extended Kalman filter, is used by an input-state feedback control law to stabilize the formation. Simulations as well as experimental results validate the theoretical results and show the effectiveness of the proposed design.

Index Terms—Mobile robots, nonlinear observability, formation control, panoramic cameras, feedback linearization.

I. INTRODUCTION

A growing interest on coordination and control of multiple autonomous agents matured in the last decade [7], [9], [15], [20]. The formation control problem has been playing an important role in this research area, giving rise to a rich literature [1], [22], [23]. By *formation control* we simply mean the problem of controlling the relative position and orientation of robots in a group while allowing the group to move as a whole. In the *leader-follower* formation control approach, a robot, the leader, moves along a predefined trajectory while the other robots, the followers, are to maintain a desired distance and orientation to it [5], [8]. Even if leader-follower architectures are known to have poor disturbance rejection properties and the over-reliance on a single agent for achieving a common goal may be undesirable, the leader follower approach is appreciated for its simplicity and scalability.

An inexpensive and challenging way to approach the formation control problem is to use exclusively passive vision sensors (off-the-shelf cameras) which provide only the projection (or view-angle) of the scene points, but not the distance.

Obviously, formation control can be achieved only if a *localization problem* has been solved, i.e. only if an estimate of the relative distance and orientation of the robots w.r.t. a common reference frame is available.

The localization problem with vision sensors is intrinsically nonlinear [4], in fact linearized approximations can be non-observable while tools from differential nonlinear systems

theory prove the possibility to reconstruct the state. Such a problem is usually referred to as the *observability of perspective dynamical systems* [12], [13] and can be embedded in the more general problem of current state estimation using input-output measurements. In [6], the state estimation for a single robot is approached using a Luenberger-like nonlinear observer, based on the projection of stationary landmarks in the environment. In [24], the localization problem for a team of nonholonomic mobile robots with calibrated vision sensors is addressed using motion segmentation techniques based on optical-flow.

This paper deals with vision-based localization and control of leader-follower formations of unicycle robots. Our work has been particularly inspired by [8], in which the authors present an interesting centralized framework for vision-based leader-follower formation control. In [8] the distance between the robots is assumed to be known and provided by the on-board fully calibrated panoramic cameras. The height of the cameras to the floor is supposed to be a priori known as well. These strong assumptions restrict the practical applicability of the control strategy in [8] to near robots.

As an original contribution, in this work we assume that each panoramic camera *only* provides the view-angle to the other robots, but not the distance, that is estimated by a nonlinear observer (the extended Kalman filter, EKF). The observability of the leader-follower system has been *analytically* studied using a new sufficient condition valid for generic nonlinear systems and based on the Extended Output Jacobian matrix. The observability condition for our system has an attractive geometrical interpretation, that allows to better understand how both the observer and the input-state feedback control law affect the formation localizability. Simulation and experimental results are presented to validate the theoretical contribution and to show the effectiveness of the proposed design.

The rest of the paper is organized as follows. In Sect. II, the leader-follower kinematic model and the assumptions on sensing and communication are presented. In Sect. III, we introduce the new observability condition based on the Extended Output Jacobian matrix. In Sect. IV, the input-state feedback control law is described. Simulations as well as experimental results are presented and discussed in Sect. V and VI. In Sect. VII the main contributions of the paper are summarized and future research directions are highlighted. The Appendix recalls some basic facts on the consistency of a state estimator.

G.L. Mariottini, F. Morbidi and D. Prattichizzo are with Dipartimento di Ingegneria dell'Informazione, University of Siena, 53100 Siena, Italy.

N. Vander Valk, N. Michael, G. Pappas and K. Daniilidis are with GRASP Laboratory, University of Pennsylvania, Philadelphia, PA 19104, USA.

Corresponding Author: Gian Luca Mariottini.

II. LEADER-FOLLOWER SETUP

A. Kinematic model

Let us consider the leader-follower setup considered in Fig. 1. The kinematics of each robot can be abstracted as a unicycle model,

$$\dot{x} = v \cos \theta, \quad \dot{y} = v \sin \theta, \quad \dot{\theta} = \omega, \quad (1)$$

where (x, y) represents the position of each robot and θ its orientation with respect to the world frame $\langle W \rangle$. The *leader* $\langle L \rangle$ has a configuration vector $[x_L \ y_L \ \theta_L]^T$ while the *follower* $\langle F \rangle$ has a vector $[x_F \ y_F \ \theta_F]^T$. The control inputs of the leader and the follower are the linear and angular velocities $[v_L \ \omega_L]^T$ and $[v_F \ \omega_F]^T$, respectively.

The whole leader-follower system can be modelled using polar coordinates, where ρ is the distance from the center of the leader to a marker P placed at a known distance d on the follower (see Fig. 1). The variable ψ is the view-angle from the y -axis of the leader to the marker P , while β is the relative orientation of the robots, i.e., $\beta \triangleq \theta_L - \theta_F$.

In the spirit of [8], [17], we introduce the following kinematic model:

Proposition 1 (Leader – follower kinematic model): With reference to Fig. 1, the leader – follower kinematic model can be written as follows:

$$\dot{\mathbf{s}} = \mathbf{G}(\mathbf{s}) \mathbf{u}, \quad (2)$$

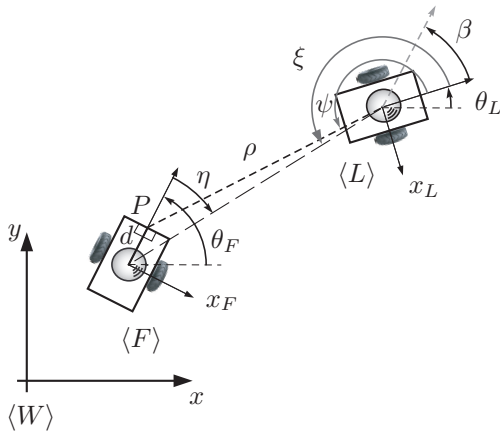


Fig. 1. Leader-follower setup in polar coordinates representation.

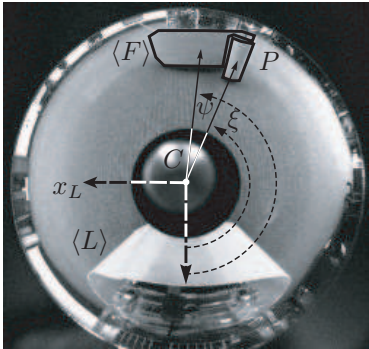


Fig. 2. View-angles computation (on the leader). HSV color blob detection is used to determine the two angles ξ and ψ from the leader to the follower's center and marker, respectively.

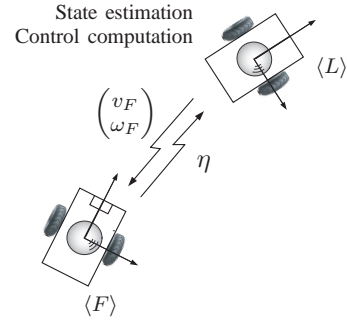


Fig. 3. The communication network and the information flow between the leader and the follower.

where $\mathbf{s} \triangleq [\rho \ \psi \ \beta]^T$, $\mathbf{u} \triangleq [v_F \ \omega_F \ v_L \ \omega_L]^T$ and

$$\mathbf{G}(\mathbf{s}) = \begin{bmatrix} \cos \gamma & d \sin \gamma & -\cos \psi & 0 \\ -\frac{\sin \gamma}{\rho} & \frac{d \cos \gamma}{\rho} & \frac{\sin \psi}{\rho} & -1 \\ 0 & -1 & 0 & 1 \end{bmatrix}$$

where $\gamma \triangleq \beta + \psi$. ■

The kinematic model in the case of q followers can be obtained by simply extending (2). In this case the input vector is $\mathbf{u} \triangleq [v_{F_1}, \omega_{F_1}, \dots, v_{F_q}, \omega_{F_q}, v_L, \omega_L]^T$ and the state vector is $\mathbf{s} \triangleq [\mathbf{s}_1^T \ \dots \ \mathbf{s}_q^T]^T \in \mathbb{R}^{3q}$ (see [17] for more details).

B. Sensing

Each robot is equipped only with an omnidirectional camera [3]. This sensor is particularly suited for mobile robot navigation, due to its field of view that is wider than that of a standard pinhole camera (Fig. 2). According to the setup in Fig. 1, $\langle L \rangle$ can measure the view-angles ξ and ψ given by the observation of the follower's centroid and the colored marker P , respectively. Analogously, the camera on $\langle F \rangle$ can measure the view-angle η to the leader.

The measurement of view-angles is obtained on each robot by means of an automatic real-time color detection and tracking algorithm [10]. Since in our setup each robot has been characterized by a specific color, leader-follower sensing association is fully automatic. More implementation details will be discussed in Sect.VI.

C. Communication

The state estimation process and the control computation are centralized on the leader, which transmits to the follower the control velocities $[v_F \ \omega_F]^T$ needed to drive the formation (Fig. 3). Due to the above assumption, the inter-robot communication is made fast because the follower will only need to transmit its view-angle η to the leader. We assume no communication delays in the view-angle transmission. From Fig. 1 is evident that β can be computed as follows:

$$\beta = -\xi + \eta + \pi. \quad (3)$$

To simplify the discussion, we will henceforth refer *only* to β , implicitly assuming the transmission of η . To summarize,

we will assume that the leader can measure a two dimensional output vector,

$$\mathbf{y} \triangleq [y_1 \ y_2]^T = [\psi \ \beta]^T. \quad (4)$$

As a concluding remark we emphasize here two original contributions which differentiate this work from [8]. First of all, we do not assume a full knowledge of camera calibration parameters. In fact, only the image center C is needed to compute the view-angles and, in many practical cases, C simply coincides with the central black hole in panoramic images (Fig. 2). Second, and most important, we assume that the leader-follower relative distance ρ in (2) is *unknown*. The problem of range estimation will be studied in detail in the next section.

III. VISION-BASED OBSERVABILITY OF LEADER-FOLLOWER FORMATIONS

A. Observability of nonlinear systems

This section reviews some basic facts about the observability of nonlinear systems [13], [14] and presents a novel and general condition (Prop. 3) that will be used to study the observability of vision-based leader-follower formations.

Consider a generic nonlinear system Σ_N of the form

$$\Sigma_N : \begin{cases} \dot{\mathbf{s}}(t) = \mathbf{f}(\mathbf{s}(t), \mathbf{u}(t)), & \mathbf{s}(0) \equiv \mathbf{s}_0 \\ \mathbf{y}(t) = \mathbf{h}(\mathbf{s}(t)) = [h_1 \ h_2 \ \dots \ h_m]^T \end{cases} \quad (5)$$

where $\mathbf{s}(t) = [s_1(t) \ s_2(t) \ \dots \ s_n(t)]^T \in \mathcal{S}$ is the state, $\mathbf{y}(t) \in \mathcal{Y}$ the observation vector and $\mathbf{u}(t) \in \mathcal{U}$ the input vector. \mathcal{S} , \mathcal{Y} and \mathcal{U} are differential manifolds of dimension n , m and p , respectively.

The problem of *observability* for Σ_N can be roughly viewed as the injectivity of the input-output map $\mathcal{R}_{\Sigma_N} : \mathcal{S} \times \mathcal{U} \mapsto \mathcal{Y}$ with respect to the initial conditions.

Two states $\mathbf{s}_1, \mathbf{s}_2$ ($\mathbf{s}_1 \neq \mathbf{s}_2$) are said *indistinguishable* [19] and denoted by $\mathbf{s}_1 \mathcal{I} \mathbf{s}_2$, if $\mathbf{y}_{\mathbf{s}_1, \mathbf{u}(t)} = \mathbf{y}_{\mathbf{s}_2, \mathbf{u}(t)}$, i.e. there exists an input $\mathbf{u}(t)$ and a time t for which, starting from different \mathbf{s}_1 and \mathbf{s}_2 , Σ_N exhibits the same outputs.

The concepts of observability and indistinguishability are tightly related, as shown in the following definition [19].

Definition 1 (Observability): Given two states $\mathbf{s}_1, \mathbf{s}_2 \in \mathcal{S}$, the system Σ_N is *observable*, if

$$\mathbf{s}_1 \mathcal{I} \mathbf{s}_2 \Rightarrow \mathbf{s}_1 = \mathbf{s}_2.$$

Given a scalar-valued function $\lambda(\mathbf{s}) : \mathbb{R}^n \mapsto \mathbb{R}$, we define the gradient operator as follows:

$$d\lambda(\mathbf{s}) \triangleq \frac{\partial \lambda(\mathbf{s})}{\partial \mathbf{s}} = \left[\frac{\partial \lambda(\mathbf{s})}{\partial s_1} \quad \frac{\partial \lambda(\mathbf{s})}{\partial s_2} \quad \dots \quad \frac{\partial \lambda(\mathbf{s})}{\partial s_n} \right].$$

The *Lie derivative* of a scalar-valued function $h(\mathbf{s})$ along a vector field $\mathbf{g} : \mathbb{R}^n \rightarrow \mathbb{R}^n$ is a real-valued function, defined as,

$$L_{\mathbf{g}} h(\mathbf{s}) \triangleq d\mathbf{h} \mathbf{g}.$$

The Lie derivative can be repeated recursively as,

$$L_{\mathbf{g}}^k h(\mathbf{s}) \triangleq L_{\mathbf{g}} [L_{\mathbf{g}}^{k-1} h(\mathbf{s})], \quad \forall k \geq 1,$$

being $L_{\mathbf{g}}^0 h(\mathbf{s}) \triangleq h(\mathbf{s})$.

For a generic nonlinear system as in (5), global or complete observability can not be usually expected and weaker notions, such that of *local weak observability* have been introduced in the literature. A sufficient condition for the observability of Σ_N has been first introduced by Hermann and Krener in [11] and is here reported for the reader's convenience.

Proposition 2 (Observability rank condition): Σ_N in (5) is said to be locally weak observable at a point $\mathbf{s}^o \in \mathcal{S}$, if there exist an open set \mathcal{D} of \mathbf{s}^o and positive integers j_1, j_2, \dots, j_m satisfying $j_1 + j_2 + \dots + j_m = n$ such that, for arbitrary $\mathbf{s} \in \mathcal{D}$, the set of row vectors defined by

$$\{L_{\mathbf{f}}^{j-1} dh_i(\mathbf{s}) \mid i = 1, \dots, m; j = 1, \dots, j_m\} \quad (6)$$

is linearly independent. \blacksquare

An equivalent and more intuitive formulation of Prop. 2 is presented and proved in what follows. It is based on the so-called Extended Output Jacobian (EOJ) matrix [6].

Proposition 3 (EOJ observability rank condition [17]):

Σ_N is said to be locally weakly observable at a point $\mathbf{s}^o \in \mathcal{S}$, if there exist an open set \mathcal{D} of \mathbf{s}^o such that, for arbitrary $\mathbf{s} \in \mathcal{D}$,

$$\text{rank}(\mathbf{J}) = n,$$

where $\mathbf{J} \in \mathbb{R}^{mn \times n}$, the Extended Output Jacobian matrix, is built by stacking the row vectors,

$$\{dh_i^{(j-1)}(\mathbf{s}) \mid i = 1, \dots, m; j = 1, \dots, n\}. \quad (7)$$

The superscript j refers to the order of time differentiation of the functions $h_i(\mathbf{s})$, $i = 1, \dots, m$.

Proof: The proof is constructive. Computing the Lie derivatives in (6), it turns out that for $i = 1, \dots, m$,

$$(j = 1) \quad L_{\mathbf{f}}^0 dh_i(\mathbf{s}) = \frac{\partial h_i(\mathbf{s})}{\partial \mathbf{s}} = dh_i^{(0)}(\mathbf{s}) \quad (8)$$

$$(j = 2) \quad L_{\mathbf{f}}^1 dh_i(\mathbf{s}) = \frac{\partial}{\partial \mathbf{s}} [L_{\mathbf{f}}^0 dh_i(\mathbf{s})] \mathbf{f}(\mathbf{s}) = d \left[\frac{\partial h_i}{\partial \mathbf{s}} \mathbf{f}(\mathbf{s}) \right] = d \left[\frac{\partial h_i}{\partial \mathbf{s}} \frac{\partial \mathbf{s}}{\partial t} \right] = dh_i^{(1)}(\mathbf{s}) \quad (9)$$

$$(j = 3) \quad L_{\mathbf{f}}^2 dh_i(\mathbf{s}) = d \left[\frac{\partial}{\partial \mathbf{s}} [L_{\mathbf{f}}^1 dh_i(\mathbf{s})] \right] = d \left[\frac{\partial h_i^{(1)}}{\partial \mathbf{s}} \dot{\mathbf{s}} \right] = d \left[\frac{\partial (\frac{\partial h_i}{\partial t})}{\partial \mathbf{s}} \frac{\partial \mathbf{s}}{\partial t} \right] = dh_i^{(2)}(\mathbf{s}) \quad (10)$$

$$\vdots \quad \quad \quad \vdots$$

$$(j = n) \quad L_{\mathbf{f}}^{n-1} dh_i(\mathbf{s}) = dh_i^{(n-1)}(\mathbf{s}) \quad (11)$$

and by stacking the vectors (8),(9),(10) and (11) in a matrix, from Prop. 2 we obtain the thesis. \blacksquare

Remark 1: Prop. 3 states that the observability of Σ_N can be tested by checking the rank of the EOJ matrix \mathbf{J} made of the state partial derivatives of the output vector and of all its $n - 1$ time derivatives. In particular, it is straightforward to verify that Σ_N is observable also when *at least one* $n \times n$ submatrix of \mathbf{J} has full rank. This simplifies the analysis, since it is not necessary to check for the determinants of all the possible submatrices of \mathbf{J} .

B. Observability of leader-follower formations

Prop. 3 is used here to determine an observability condition for the leader-follower system described in Sect. II.

From Prop. 3, the observability of (2) with output (4), is guaranteed when at least one 3×3 submatrix of the whole 6×3 EOJ matrix is nonsingular. Let us consider, e.g. the submatrix $\bar{\mathbf{J}}$:

$$\bar{\mathbf{J}} = \begin{bmatrix} \frac{\partial y_1}{\partial \rho} & \frac{\partial y_1}{\partial \psi} & \frac{\partial y_1}{\partial \beta} \\ \frac{\partial y_2}{\partial \rho} & \frac{\partial y_2}{\partial \psi} & \frac{\partial y_2}{\partial \beta} \end{bmatrix} = \begin{bmatrix} 0 & 1 & 0 \\ 0 & 0 & 1 \end{bmatrix}, \quad (12)$$

whose determinant is,

$$\det(\bar{\mathbf{J}}) = -\frac{\partial \dot{\psi}}{\partial \rho} = \frac{1}{\rho} [\dot{\psi} + \omega_L]. \quad (13)$$

Therefore, if $\dot{\psi} + \omega_L \neq 0$, the state \mathbf{s} is observable.

In the case of $q > 1$ followers, the observability condition is a simple extension of (13) (see [17]).

C. A geometrical interpretation of the EOJ singularity

In Fig. 4 we provide a basic example to give some geometrical interpretation of (13). A leader and two followers are considered at two different time instants, $t = 0$ and $t = 1$. All the robots move with the same translational velocity and zero angular velocity.

We first note that that $\psi_2(1) \neq \psi_2(0)$ (and thus $\dot{\psi}_2 \neq 0$) due to the different initial orientation between $\langle L \rangle$ and $\langle F_2 \rangle$. Then, from (13), it turns out that the state \mathbf{s}_2 is observable. This is intuitively correct, since the visual information varies in time and it is then expected to improve the localizability. This leads also to the intuition that curvilinear trajectories have a favourable effect on observability, since a change of the output signal (4) occurs there.

From an inspection of Fig. 4, it is also evident that there is not any improvement in the localization between $\langle L \rangle$ and $\langle F_1 \rangle$ since their relative motion is zero from $t = 0$ to $t = 1$ (and thus $\dot{\psi}_1 = 0$). Recall that Prop. 2 only provides a sufficient condition for observability and that $\det(\bar{\mathbf{J}}) = 0$ does not necessarily imply that the state \mathbf{s}_1 is not observable. However, the simulation and experimental results reported in Sect. V and Sect. VI will give us the strong evidence that a singular EOJ matrix can be used as an index of non-observability.

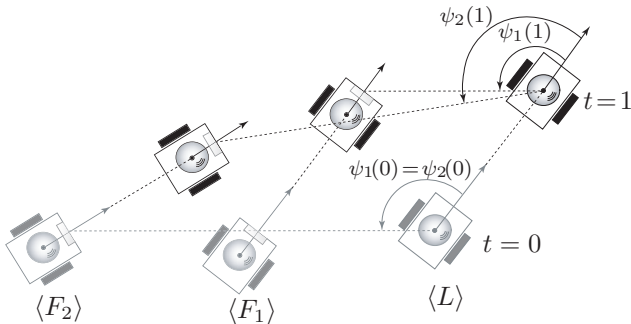


Fig. 4. Geometrical interpretation of the EOJ singularity.

D. Observer design

In order to control the formation, an estimate $\hat{\mathbf{s}}$ of the state configuration \mathbf{s} is required. An extended Kalman filter has been designed to estimate the range ρ given the input vector \mathbf{u} and the outputs \mathbf{y} . We assume additive noise on both the process and measurement equations,

$$\dot{\mathbf{s}} = \mathbf{G}(\mathbf{s}) \mathbf{u} + \mathbf{z} \quad (14)$$

$$\mathbf{y} = \mathbf{C} \mathbf{s} + \mathbf{v} \quad (15)$$

where \mathbf{C} is the output transition matrix and \mathbf{z} and \mathbf{v} are zero mean white gaussian noises with covariance matrices \mathbf{Q} and \mathbf{R} , respectively. $\mathbf{s}(0)$, \mathbf{z} and \mathbf{v} are assumed to be uncorrelated. Equation (14) has been discretized using the Euler forward method with sampling time T_c ,

$$\mathbf{s}(k+1) = \mathbf{\Gamma}(\mathbf{s}(k), \mathbf{u}(k)) + T_c \mathbf{z}$$

where $\mathbf{\Gamma}(\mathbf{s}(k), \mathbf{u}(k)) \triangleq T_c \mathbf{G}(\mathbf{s}) \mathbf{u} + \mathbf{s}(k)$ and $k \in \mathcal{N}$. As we will see in Sect.V, the EKF exhibits good performances in estimating the distance ρ in both the simulations and the experiments we conducted to test the robustness of our approach.

IV. INPUT-STATE FEEDBACK CONTROL

Consider the set of kinematic equations equivalent to (2):

$$\dot{\mathbf{s}}_r = \mathbf{F}(\mathbf{s}) \mathbf{u}_L + \mathbf{H}(\mathbf{s}) \mathbf{u}_F \quad (16)$$

$$\dot{\beta} = \omega_L - \omega_F \quad (17)$$

where $\mathbf{s}_r \triangleq [\rho \ \psi]^T$ is a *reduced* state-space vector. Matrices \mathbf{H} and $\mathbf{F} \in \mathbb{R}^{2 \times 2}$ are the two upper left and right 2×2 minors of \mathbf{G} , respectively.

In the spirit of [8], we propose here an input state feedback control law for the robot formation. Let us consider the following control input

$$\mathbf{u}_F \triangleq [v_F \ \omega_F]^T = \mathbf{H}^{-1}(\mathbf{s})(\mathbf{p} - \mathbf{F}(\mathbf{s}) \mathbf{u}_L) \quad (18)$$

where

$$\mathbf{p} = \dot{\mathbf{s}}_r^{des} - \mathbf{K}(\mathbf{s}_r - \mathbf{s}_r^{des}) \quad (19)$$

where $\mathbf{K} = \text{diag}\{k_1, k_2\}$, with $k_1, k_2 > 0$. The superscript “*des*” refers to the desired values. Equation (18) acts in (16) as a feedback linearizing control, so that the closed-loop dynamics become,

$$\dot{\mathbf{s}}_r = \dot{\mathbf{s}}_r^{des} - \mathbf{K}(\mathbf{s}_r - \mathbf{s}_r^{des}), \quad \dot{\beta} = \omega_L - \omega_F. \quad (20)$$

The following proposition states that it suffices to control \mathbf{s}_r towards \mathbf{s}_r^{des} using (18), to guarantee the local stability of the whole state-space vector \mathbf{s} .

Proposition 4: Let us suppose that $v_L > 0$, $|\omega_L| < W_{max}$, $|\beta(0)| < \pi$ and that $\dot{\mathbf{s}}_r^{des}$ is bounded. Then the control law (18)-(19) stabilizes the system dynamics (16)-(17).

Proof: Let us refer to $[e_\rho \ e_\psi]^T = \mathbf{s}_r - \mathbf{s}_r^{des}$ as the state tracking error vector. From (20), it follows that $[e_\rho \ e_\psi]$ is globally exponentially stable. We now prove that the internal

dynamics is stable, i.e., that $|\beta|$ is bounded. Drawing ω_F from (18), equation (17) can be rewritten as:

$$\dot{\beta} = -\frac{\sin \gamma}{d}(\dot{\rho}^{des} - k_1 e_\rho) - \frac{\rho \cos \gamma}{d}(\dot{\psi}^{des} - k_2 e_\psi) - \frac{v_L}{d} \sin \beta - \omega_L \left(\frac{\rho}{d} \cos \gamma - 1 \right). \quad (21)$$

Due to the physical constraints of the robots, we can reasonably assume that ω_L is bounded. Moreover, if also $\dot{\psi}^{des}$ and $\dot{\rho}^{des}$ are bounded, then (21) can be re-written as:

$$\dot{\beta} = -\frac{v_L}{d} \sin \beta - B(t). \quad (22)$$

Note that without the term $B(t)$, a bounded persistent disturbance, (22) is *locally* asymptotically stable for $|\beta| < \pi$. From the stability theory of nonlinear systems with persistent disturbances [21], being $|\beta(0)| < \pi$ and $B(t)$ bounded, it follows that $|\beta(t)| < \varepsilon, \forall t > T$, for finite time T and $\forall \varepsilon > 0$. ■

Remark 2 (Distant robots): If the distance between the leader and follower is *big*, it is in general difficult to exactly locate the marker P in the image (recall Sect. II-B and Fig. 2). A possible solution consists in detecting *only* the robot centroid, that is equivalent to assume $d = 0$. Even though this assumption does not affect the observability condition presented in Sect. III-B, however it has a negative influence on the control. In fact $\mathbf{H}(\mathbf{s})$ is singular when $d = 0$ and the control in (18) is not applicable. In [16], a possible solution is presented with a feedback control based on dynamic extension that overcomes this control issue.

V. SIMULATION RESULTS

This section presents the simulation experiments we conducted to test the effectiveness of the proposed formation control strategy. The simulations gave us also the evidence that a singular EOJ matrix can be used as an index of non-observability.

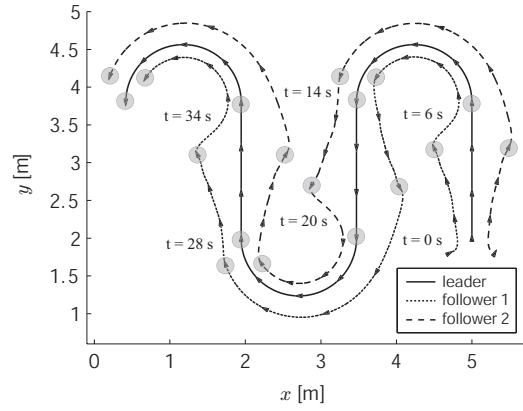
The following velocity input was assigned to the leader,

$$v_L(t) = 0.3 \text{ m/s}$$

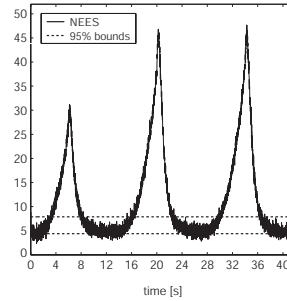
$$\omega_L(t) = \begin{cases} 0 \text{ rad/s} & \text{if } t \in \{[0, 6], (14, 20], (28, 34]\} \\ \pi/8 \text{ rad/s} & \text{otherwise,} \end{cases}$$

which undergoes a piecewise rectilinear-circular trajectory that is particularly suited for testing the condition (13), according to the geometrical interpretation in Sect. III-C. The formation considered in the simulation experiments consists of two followers. We set $\mathbf{s}(0) = [0.261 \ 2.183 \ 1.047 \ 0.368 \ 4.399 \ 0.524]^T$ and $\mathbf{s}_r^{des} = [0.3 \ 3\pi/4 \ 0.3 \ 5\pi/4]^T$, where distances are in meters and angles in radians.

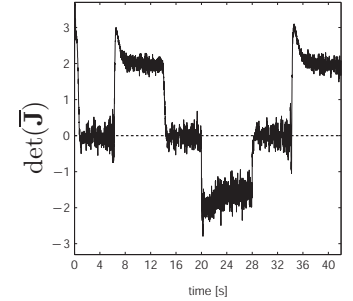
The gain matrix of the controller is $\mathbf{K} = 6 \mathbf{I}_4$, where \mathbf{I}_4 denotes the 4×4 identity matrix. The EKF was initialized with $\hat{\mathbf{s}}(0| - 1) = [\frac{3}{2}\rho_1(0) \ \psi_1(0) \ \beta_1(0) \ \frac{3}{2}\rho_2(0) \ \psi_2(0) \ \beta_2(0)]^T$ corresponding to a 50% perturbation of the unknown distances to the leader and covariance matrix $\mathbf{P}(0| - 1) = 10^{-2} \cdot \text{diag}\{1, 1.1, 1.1, 1, 1.1, 1.1\}$. The other parameters are $T_c = 10$ ms, $d = 0.1$ m, $\mathbf{Q} = \text{diag}\{3 \cdot 10^{-5}, \varrho, \varrho, 3 \cdot 10^{-5}, \varrho, \varrho\}$ and $\mathbf{R} = \varrho \mathbf{I}_4$, where



(a)



(b)



(c)

Fig. 5. Simulation results: (a) Trajectory of the robots; (b) Time history of NEES and 95% bounds ($N = 15$); (c) Time history of $\det(\bar{\mathbf{J}})$.

$\varrho = 0.9187 \cdot 10^{-4} \text{ rad}^2$. White gaussian noise is added to the measurements.

Fig. 5(a) shows the trajectory of the three robots (in order to have a temporal reference the vehicles are drawn every two seconds). It is evident that the followers miss the formation exactly along the rectilinear tracts of the trajectory (e.g. in $t \in (14, 20]$) where visual data are not changing sensibly so as to improve the localization process. On the other hand, when the leader switches from the rectilinear to the curvilinear tracts (e.g. in $t \in (20, 28]$), a change in the visual information occurs and this leads to an improvement of the localization: the desired formation is in fact immediately recovered. The consistency of the EKF is studied in Fig. 5(b) where a concise representation of the estimation error, the time history of NEES (see the Appendix), is provided (here $r_1 = 4.38$, $r_2 = 7.87$ and $N = 15$). Comparing Fig. 5(a) with Fig. 5(b), it is evident that the NEES tends to leave the 95% bounds exactly in correspondence of the rectilinear tracts of the leader trajectory (e.g. in $t \in (14, 20]$).

Fig. 5(c) reports the time history of $\det(\bar{\mathbf{J}})$. Note that $\bar{\mathbf{J}}$ is relative to follower 1: similar results are obtained when the $\bar{\mathbf{J}}$ relative to the follower 2 is considered. According to condition (13), we see that the state \mathbf{s}_1 (analogously \mathbf{s}_2) is observable along the curvilinear tracts of the trajectory, i.e. where $\det(\bar{\mathbf{J}}) \neq 0$. More interestingly, note that $\det(\bar{\mathbf{J}})$ is near zero in the time intervals in which the NEES increases,

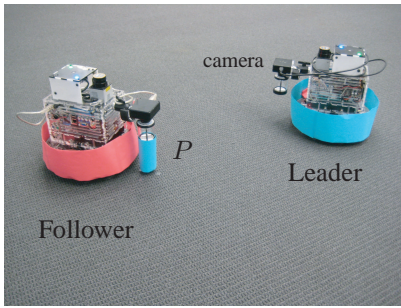


Fig. 6. Experimental setup. The *Scarab* robots used in the experiments.

meaning that the state s_1 (analogously s_2) is not observable there. Even though further theoretical investigations are needed to confirm this result, this empirical evidence makes us conjecture that Prop. 3 is both necessary and sufficient, i.e. that the singularity of the EOJ matrix can be used as an index of non-observability.

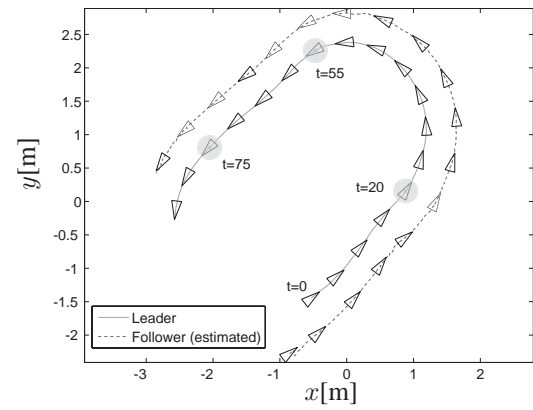
VI. EXPERIMENTS

In order also to validate the proposed formation control strategy in a real scenario, some experiments have been carried out at the GRASP Lab, University of Pennsylvania, Philadelphia. The experimental setup consists of two *Scarab* robots acting as the leader and the follower (see Fig. 6).

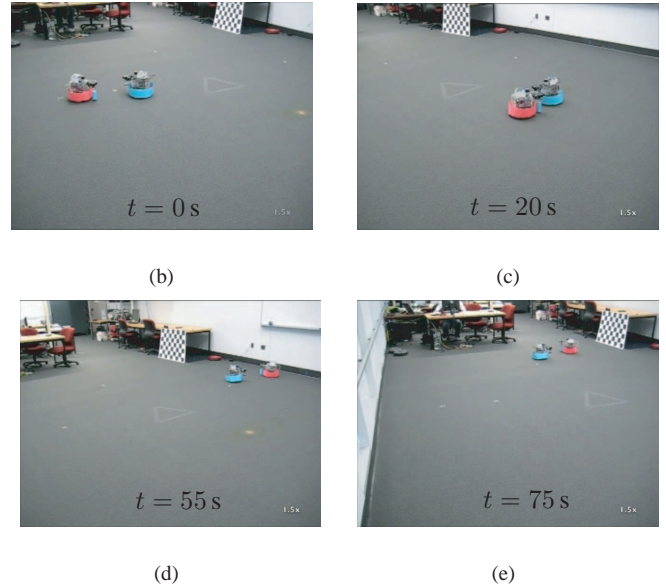
The *Scarab* is a differential driven robotic platform designed at the GRASP Lab, measuring $20 \times 13.5 \times 22.2$ cm³. The leader and the follower run identical modularized software with well-defined interfaces connecting modules via the Player robot architecture system. In order to provide a ground truth information of the actual robots pose, a tracking system consisting of LED markers on the top of each robot and eight overhead cameras are employed. More technical details on the *Scarab* robots and on the tracking system can be found in [18].

Each robot is uniquely identified by a colored marker and equipped with a panoramic camera, consisting of a hyperbolic Remote Reality mirror (folded) screwed on a Point Grey Firefly IEEE 1394 camera. The image resolution is 320×240 pixels. Only the image principal point (u_0, v_0) is known and is given by $(159.48, 123.70)$ pixels and $(172.89, 126.53)$ pixels, for the leader and the follower's camera, respectively. HSV color blob detection is run on each robot using the Intel's OpenCV libraries. Though many other techniques are available in the literature (e.g. optical-flow, corner detection, etc.), we experienced good real-time performances and robustness of our code to changing in illumination, to partial occlusions and also to the tracking of far robots. The distance between the center of the robot and the marker is $d = 20$ cm.

Note that, due to the presence of the LED marker on the top of each robot, the position of the panoramic camera on the vehicles is different from that shown in Fig. 1. However, a simple algebraic transformation is sufficient to readapt the robots' angle measurement to the model in Fig. 1. This transformation has been implemented in the code running on the robots without significantly affecting the performance and the computational burden.



(a)



(b)

(c)

(d)

(e)

Fig. 7. Experimental results. (a) Trajectory of the leader and the follower. The time instants in which the leader switches from the rectilinear to the circular tracks and viceversa, are highlighted. (b)-(e) Snapshots from the experiment.

For the experiment, we chose $s(0) = \hat{s}(0| - 1) = [0.75 \text{ m}, 5/4\pi \text{ rad}, 0]^T$ and $s_r^{des} = [0.5 \text{ m}, 5/4\pi \text{ rad}]^T$. The control gains are $k_1 = k_2 = 0.5$ and $T_c = 0.1$ s. Moreover, $\mathbf{P}(0| - 1) = 10^{-2} \cdot \mathbf{I}$, $\mathbf{Q} = 10^{-5} \cdot \text{diag}\{3, 9, 9\}$ and $\mathbf{R} = 10^{-5} \cdot \text{diag}\{9.1, 9.1\}$.

As in Sect. V, we selected an input vector $[v_L, w_L]^T$ giving rise to a rectilinear/circular trajectory.

Fig. 7(a) shows the trajectory of the robots during the whole experiment¹, from which it can be seen that the follower succeeds in attaining the desired formation. We highlighted the time instants in which the leader switches from the linear to the curvilinear trajectory, and viceversa. A series of snapshots from the experiment is reported in Figs. 7(b)-7(e). The range estimation error $\rho - \hat{\rho}$ and the range tracking error $\rho^{des} - \hat{\rho}$ are shown in Fig. 8(a) and Fig. 8(b), respectively. Note that, as expected from the theory (see Sect. III-C), the estimation and tracking errors decrease and stay close to zero approximately

¹A video of the experiments can be downloaded at www.dii.unisi.it/~gmariottini/VisionLocalizationMultirobot.m4v.

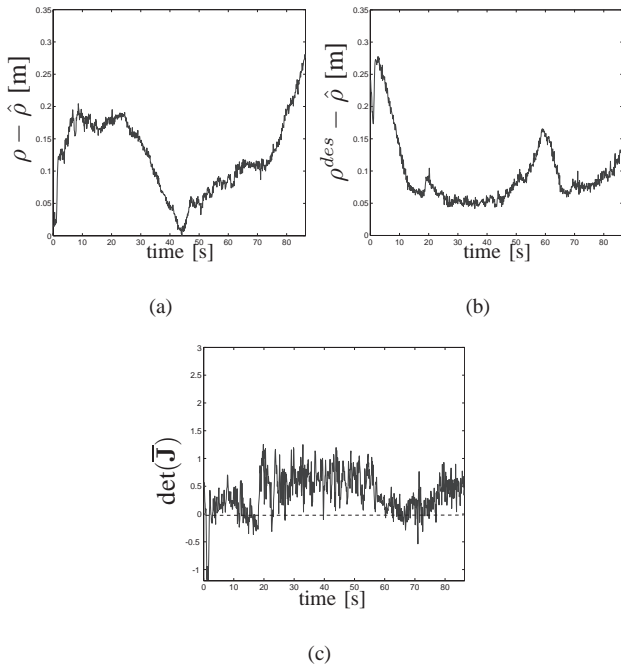


Fig. 8. Experimental results. Time history of (a) the observation error; (b) the control error; (c) $\det(\bar{J})$.

in $t \in [20, 55]$, that is during the circular trajectory. Moreover, in confirmation of the simulation results of Sect. V, the EOJ matrix is close to singularity approximately at the same time instants in which the tracking and estimation errors increase, that is when the leader moves along the rectilinear tracts (see Fig. 8(c)).

VII. CONCLUSIONS AND FUTURE WORK

This paper studies the vision-based localization and control of a leader-follower formation of nonholonomic mobile robots. Each robot is equipped with a panoramic camera which only provides the view-angle to the other vehicles. The vision-based formation localizability problem is addressed using a new sufficient observability condition based on the Extended Output Jacobian matrix. The state of the leader-follower system is estimated via the extended Kalman filter and an input-state feedback control law is designed to stabilize the formation. Simulations as well as real-data experiments performed with Scarab robots illustrate the theory and show the effectiveness of the proposed design.

The comparison between the extended Kalman filter and other state estimators (such as, e.g. the unscented Kalman filter, particle filters, etc.) is the subject of on-going research and will be addressed in future works. Future research is also involved in extending our results to vehicles with more involved kinematics (such as e.g., car-like robots).

ACKNOWLEDGEMENTS

This research was supported under the grants NSF-EIA-0324977, NSF-IIS-0713260, NSF-IIP-0742304, and ARO/MURI DAAD19-02-1-0383, Fondazione MPS 2005.

APPENDIX CONSISTENCY OF A STATE ESTIMATOR

Definition 2: A state estimator is said to be *consistent* [2] if its state estimation error $\tilde{s}(k|k) \triangleq \hat{s}(k) - s(k|k)$ is such that $E[\tilde{s}(k|k)] = \mathbf{0}$ and $E[\tilde{s}(k|k)\tilde{s}(k|k)^T] = \mathbf{P}(k|k)$.

To practically evaluate the consistency of an estimator, the *normalized estimation error squared* (NEES) is defined:

$$\varepsilon(k) \triangleq \tilde{s}(k|k)^T \mathbf{P}^{-1}(k|k) \tilde{s}(k|k).$$

Let us consider N Monte Carlo simulations that provide N samples $\varepsilon_i(k)$ of the random variable $\varepsilon(k)$. Let $\bar{\varepsilon}(k) = \frac{1}{N} \sum_{i=1}^N \varepsilon_i(k)$ be the sample mean of $\varepsilon(k)$. The hypothesis that the state estimation errors are consistent with the estimator calculated covariances is not invalidated if $\bar{\varepsilon}(k) \in [r_1, r_2]$, $r_1, r_2 \in \mathbb{R}$.

Under the Gaussian assumption, $N\bar{\varepsilon}(k) \sim \chi_{N \cdot 3q}^2$ where $\chi_{N \cdot 3q}^2$ is a $N \cdot 3q$ degrees of freedom Chi-square distribution. r_1, r_2 can then be computed from a table providing the points on the Chi-square distribution for a given tail probability (see, e.g. Appendix C in [2]).

It is worth noting that even if specifically designed for linear systems, the consistency criterion based on the NEES is commonly used also in the nonlinear case.

REFERENCES

- [1] T. Balch and R.C. Arkin. Behavior-based formation control for multi-robot teams. *IEEE Trans. Robot. Autom.*, 14(6):926–939, 1998.
- [2] Y. Bar-Shalom, X.R. Li, and T. Kirubarajan. *Estimation with Applications to Tracking and Navigation*. John Wiley & Sons, 2001.
- [3] R. Benosman and S.B. Kang. *Panoramic Vision: Sensors, Theory and Applications*. Springer Verlag, New York, 2001.
- [4] A. Bicchi, D. Prattichizzo, A. Marigo, and A. Balestrino. On the observability of mobile vehicles localization. In *Proc. IEEE Mediterrean Conf. on Control and Systems*, 1998.
- [5] L. Consolini, F. Morbidi, D. Prattichizzo, and M. Tosques. Steering hierarchical formations of unicycle robots. In *Proc. 46th IEEE Conf. Decision and Control*, pages 1410–1415, 2007.
- [6] F. Coticelli, A. Bicchi, and A. Balestrino. Observability and nonlinear observers for mobile robot localization. In *Proc. IFAC Int. Symp. on Robot Control, SyRoCo, 2000*.
- [7] J. Cortés, S. Martínez, T. Karatas, and F. Bullo. Coverage control for mobile sensing networks. *IEEE Trans. Robot. Autom.*, 20(2):243–255, 2004.
- [8] A.K. Das, R. Fierro, V. Kumar, J.P. Ostrowsky, J. Spletzer, and C. Taylor. A vision-based formation control framework. *IEEE Trans. on Robot. and Autom.*, 18(5):813–825, 2002.
- [9] K.D. Do and J. Pan. Nonlinear formation control of unicycle-type mobile robots. *Robot. and Autonom. Syst.*, 55:191–204, 2007.
- [10] D.A. Forsyth and J. Ponce. *Computer Vision: A Modern Approach*. Prentice Hall, 2002.
- [11] R. Hermann and A. Krener. Nonlinear controllability and observability. *IEEE Trans. on Automat. Contr.*, AC-22:728–740, 1977.
- [12] J.P. Hespanha. State estimation and control for systems with perspective outputs. In *Proc. 41st IEEE Conf. on Decision and Control*, volume 2, pages 2208 – 2213, 2002.
- [13] H. Inaba, A. Yoshida, R. Abdursul, and B.K. Ghosh. Observability of Perspective Dynamical Systems. In *Proc. 39th IEEE Conf. on Decision and Control*, pages 5157–5162, 2000.
- [14] A. Isidori. *Nonlinear Control Systems*. Springer, 3rd edition, 1995.
- [15] J. Lin, A.S. Morse, and B.D.O. Anderson. The Multi-Agent Rendezvous Problem. In *Proc. 42nd IEEE Conf. Decision and Control*, pages 1508–1513, 2003.
- [16] G.L. Mariottini, F. Morbidi, D. Prattichizzo, G.J. Pappas, and K. Daniilidis. Leader-Follower Formations: Uncalibrated Vision-Based Localization and Control. In *Proc. IEEE Int. Conf. on Robotics and Automation*, pages 2403–2408, 2007.

- [17] G.L. Mariottini, G.J. Pappas, D. Prattichizzo, and K. Daniilidis. Vision-based localization of leader-follower formations. In *Proc. 44th IEEE Conf. on Decision and Control*, pages 635–640, 2005.
- [18] N. Michael, J. Fink, and V. Kumar. Experimental testbed for large multirobot teams. *IEEE Robot. Autom. Mag.*, 15(1):53–61, 2008.
- [19] H. Nijmeijer and A.J. van der Shaft. *Nonlinear dynamical control systems*. Springer, 1990.
- [20] W. Ren, R.W. Beard, and E.M. Atkins. A Survey of Consensus Problems in Multi-agent Coordination. In *Proc. American Control Conf.*, pages 1859–1864, 2005.
- [21] J. E. Slotine and W. Li. *Applied Nonlinear Control*. Prentice-Hall, 1991.
- [22] P. Tabuada, G.J. Pappas, and P. Lima. Motion Feasibility of Multi-Agent Formations. *IEEE Trans. Robot.*, 21(3):387–391, 2005.
- [23] K.H. Tan and M.A. Lewis. High Precision Formation Control of Mobile Robots using Virtual Structures. *Autonomous Robots*, 4(4):387–403, 1997.
- [24] R. Vidal, O. Shakernia, and S. Sastry. Following the flock: Distributed formation control with omnidirectional vision-based motion segmentation and visual servoing. *IEEE Robot. Autom. Mag.*, 11(4):14–20, 2004.